DEVELOPMENT OF BRAIN TISSUE SWELLING PREDICTIVE TOOLS FOR ISCHAEMIC STROKE PATIENT POST-TREATMENT

(PEMBINAAN ALATAN PERAMALAN PEMBENGKAKAN TISU OTAK UNTUK PESAKIT STROK ISKEMIA PASCARAWATAN)

MOHD JAMIL MOHAMED MOKHTARUDIN

AHMED NURYE OUMER

MOHD AZRUL HISHAM MOHD ADIB

MUHAMMAD HILMI JALIL

EINLY LIM

AHMAD HAFIZ ZULKIFLY

RESEARCH VOTE NO:

RDU1703310

Fakulti Teknologi Kejuruteraan Mekanikal Dan Automotif

Universiti Malaysia Pahang

2019

Acknowledgement

I would like to thank all of the members of this research grants for their expert advice and encouragement throughout this difficult project. Also, thank you to all students that are directly or indirectly involved in completing this research project.

Abstract

Ischaemic stroke is one of the causes of death worldwide. Treatments such as thrombolysis and catheterisation must be given within 3 hours after stroke onset, in which treatments beyond this time may pose risk of brain tissue swelling. Thus, a prediction system must be made to determine the suitability of a stroke treatment to avoid the risk of failure. In this report, a mathematical model based on poroelastic theory and asymptotic expansion homogenization has been developed to study the formation of brain tissue swelling after ischaemia-reperfusion treatment.

Firstly, the mathematical model of brain tissue swelling after ischaemia-reperfusion treatment is investigated using an ideal 2D brain geometry. The objective here is to observe the effect of infarct size and location towards the formation and severity of brain herniation, which will form due to brain tissue swelling. However, this model assumed that the blood pressure is constant and homogeneous throughout the brain, while in fact, the blood capillaries vary in sizes and shapes. Therefore, asymptotic expansion homogenization technique is applied to allow for the inclusion of capillaries sizes into the initial model. This method transforms the initial model into two types of equations: (1) macroscale governing equations; and (2) microscale cell problems. In order to solve for the macroscale governing equations, the microscale cell problems must first be solved on a brain tissue geometry to calculate the effective parametric tensors, which later be used in the macroscale governing equations. Lastly, the mathematical model is solved in a realistic brain geometry to evcaluate the effect of different mechanical properties of the brain towards brain tissue swelling formation.

Abstrak

Strok iskemia ialah salah satu penyebab kematian di dunia. Rawatan-rawatan seperti trombolisis dan pengkateterisasi mesti diberikan dalam masa 3 jam selepas berlakunya strok, di mana rawatan selepas tempoh masa ini mungkin berisiko untuk menyebabkan pembengkakan tisu otak. Oleh itu, satu sistem peramalan mesti dibina untuk menentukan kesesuaian suatu rawatan strok bagi mengelakkan risiko kegagalan rawatan itu. Di dalam laporan ini, satu model matematik berdasarkan teori poroelastik and penghomogenisasi pengembangan asimptotik telah dibina untuk mengkaji pembentukan pembengkakan tisu otak selepas rawatan reperfusi-iskemia.

Pertama, model matematik untuk pembengkakan tisu otak selepas rawatan reperfusi-iskemia dikaji menggunakan geometri ideal otak 2D. Objektif kajian ini ialah untuk melihat kesan saiz dan lokasi infark terhadap pembentukan dan keterukan herniasi otak, dimana ia akan terbentuk disebabkan oleh pembengkakan tisu otak. Walaubagaimanapun, model ini mengandaikan bahawa tekanan darah ialah malar dan homogeneous di keseluruhan otak, di mana secara faktanya, kapilari darah mempunyai pelbagai saiz dan bentuk. Oleh itu, teknik penghomogenisasi pengembangan asimptotik telah digunakan bagi mengambilkira kepelbagaian saiz kapilari dalam model awal ini. Metod ini mengubah model awal ini kepada dua jenis persamaan: (1) persamaan makroskala; dan (2) masalah sel mikroskala. Bagi menyelesaikan persamaan makroskala, persamaan sel mikroskala mestilah diselesaikan terlebih dahulu menggunakan geometri tisu otak untuk mengira tensor-tensor parameter efektif, di mana akan digunakan di dalam persamaan makroskala. Akhir sekali, model matematik ini diselesaikan menggunakan geometri otak yang realistik untuk menaksir kesan perbezaan sifat mekanikal otak terhadap pembentukan pembengkakan tisue otak.

Contents

List of Publications

Peer-reviewed journal articles

- M. J. M. Mokhtarudin, A. Shabudin, and S. J. Payne, "Effects of brain tissue mechanical and fluid transport properties during ischaemic brain oedema: A poroelastic finite element analysis," 2018 IEEE-EMBS Conference on Biomedical Engineering Sciences (IECBES), Sarawak, Malaysia, 2018, pp. 1-6. Doi: 10.1109/IECBES.2018.8626659.
- Shabudin, M. J. M. Mokhtarudin, S. J. Payne, and N. A. N. Mohamed, "Application of Asymptotic Expansion Homogenization for Vascularized Poroelastic Brain Tissue," 2018 IEEE-EMBS Conference on Biomedical Engineering Sciences (IECBES), Sarawak, Malaysia, 2018, pp. 413-418. Doi: 10.1109/IECBES.2018.8626727.

Conference articles

- Mohamed Mokhtarudin, M. J., Shabudin, A., and Payne, S. J. (2018, November), Brain tissue swelling during ischaemia-reperfusion: 2d finite element analysis using poroelasticity. Paper presented at 4th International Conference on Science, Engineering & Environment (SEE), Nagoya, Japan.
- Mohamed Mokhtarudin, M. J., Shabudin, A., and Payne, S. J. (2018, December), Effects of brain tissue mechanical and fluid transport properties during ischaemic brain oedema: A poroelastic finite element analysis. Paper presented at 2018 IEEE-EMBS Conference on Biomedical Engineering Sciences (IECBES), Sarawak, Malaysia.
- Shabudin, A., Mohamed Mokhtarudin, M. J., Payne, S. J., and Nik Mohamed, N. A. (2018, December), Application of Asymptotic Expansion Homogenization for Vascularized Poroelastic Brain Tissue. Paper presented at 2018 IEEE-EMBS Conference on Biomedical Engineering Sciences (IECBES), Sarawak, Malaysia.
- Mohamed Mokhtarudin, M. J., Nadzri, A. N., and Payne, S. J., (2019, June), Finite element poroelastic modelling of brain oedema formation after ischaemic stroke reperfusion. Paper presented at 6th International Conference on Computational and Mathematical Biomedical Engineering (CMBE2019), Tohoku, Japan.

List of Figures

List of Abbreviations

AEH	Asymptotic expansion homogenization
AQP4	Aquaporin-4
BBB	Blood-brain barrier
CT	Computed tomography
ICP	Intracranial pressure
MRI	Magnetic resonance imaging
MSTM	Modified spanning tree method
PDE	Partial differential equation
UMMC	University Malaya Medical Centre

Chapter 1: Introduction

1.1. Problem Statement

Brain tissue swelling is the most common risk of reperfusion treatment on ischaemic stroke [1] with about 80% mortality rate [2]. Brain tissue swelling causes the shift of the structure in the midline of the brain such as the brain ventricles. This is known as brain herniation [3], which usually occurs in about 78% of stroke patients [2]. The herniation may cause the compression of cerebral microvessels, which has been hypothesised to cause secondary stroke. Therefore, the efficacy of reperfusion treatment after stroke remains questionable because of the risk of brain tissue swelling occurrence.

A mathematical model has been developed to study the formation of brain tissue swelling after reperfusion treatment [4]. This model has been used to predict the formation of brain tissue swelling several days after the stroke patients have been discharged from the hospital. The predictions made allow the patients to avoid undergoing recurrence medical imaging procedures such as MRI and CT scanning, which are expensive and can affect the health conditions of the patients. In addition, predicting brain tissue swelling also allows the clinicians to decide on the suitable treatments such as decompression surgery [5] and osmotherapy [6]. These treatments pose several complications such as swelling through the surgical site [7] and the effectiveness have yet been clinically proven [8]. Thus, to avoid these complications, a thorough evaluation of the potentiality of the brain tissue swelling effect must be done.

The development of predictive tools for brain tissue swelling must meet these criteria: (1) the model must be simple yet informative; and (2) the model must be validated with clinical data. A simplify model can be developed using mathematical techniques such as multiscale modelling, which simplifies a model that requires information from

various scales exist in the physics. After the mathematical model has been developed, it must be validated using medical imaging data. The data will be collected from University Malaya Medical Centre (UMMC). The predictive tools are intended to be used by neurosurgeon in improving their decision-making in providing treatments to ischaemic stroke patients.

1.2. Research Objective

The objective of this project is divided into three:

1. To modify the existing mathematical model for brain tissue swelling using multiscale modelling technique;
2. To simulate the existing and modified mathematical model in 2D and 3D environment using finite element analysis; and
3. To validate the mathematical model using patient-specific geometry developed from medical imaging data.

1.3. Research Scope

The scope of research is narrowed down as follows:

1. The simulations will be performed on an ideal geometry to test and optimize the mathematical model developed; and
2. The patient-specific geometry will be developed using medical imaging data obtained from UMMC.

1.4. Thesis Organization

The subsequent chapters in this thesis will be adapted directly from published technical papers as part of the requirements for this research grant. The thesis will be further divided into 4 chapters as follows:

1. Chapter 2: Brain tissue swelling during ischaemia-reperfusion: 2d finite element analysis using poroelasticity
2. Chapter 3: Application of asymptotic expansion homogenization for vascularized poroelastic brain tissue
3. Chapter 4: Effects of brain tissue mechanical and fluid transport properties during ischaemic brain oedema a poroelastic finite element analysis
4. Chapter 5: Conclusion and future work

Chapter 2: Brain tissue swelling during ischaemia-reperfusion: 2D finite element analysis using poroelasticity

2.1. Introduction

Brain oedema formation due to cerebral ischaemia-reperfusion can be observed using medical imaging modalities such as CT and MRI scans by the movement of brain midline structures (also known as brain herniation) or by brain tissue swelling. Herniation usually results in the compression of brain ventricle and cerebral microvessels, which further results in the occurrence of secondary ischaemia [9]. The presence of herniation may indicate the rise in the intracranial pressure (ICP) and it may cause permanent neurological problems and even fatality [10]. Several treatments are available for brain oedema such as decompressive surgery and osmotherapy. However, the effectiveness of these treatments remains questionable due to the complicated nature of brain oedema formation.

A mathematical model has been developed to further understand the formation of brain tissue swelling due to BBB breakdown using poroelastic theory. Poroelasticity was initially used to study soil mechanics [11] and has been extensively used to study the mechanics of the pathological brain [12-14]. In this theory, the brain tissue is assumed to be homogeneous, has linear elastic property, and contain both water and blood, permeable in a solid porous matrix structure. A comprehensive mathematical framework of this theory can be found in [4].

In this chapter, a mathematical model of brain tissue swelling after a cerebral ischaemia-reperfusion treatment is investigated using an ideal 2D brain geometry and solved using finite element scheme of poroelastic model. The objective here is to observe the effect of infarct size and location towards the formation and severity of brain

herniation. This will be a preliminary study before a more complete validation using MRI data of ischaemic stroke patient can be done.

2.2. Methodology

2.2.1. Theoretical Background

During ischaemic stroke, the lack of oxygen and nutrient to the affected region creates a series of biochemical reactions that destroys the endothelial cells surrounding the cerebral microvessels leading to the blood-brain barrier (BBB) breakdown, which increases the BBB permeability [15]. When blood flow is restored after reperfusion treatment, ions and some protein plasma can filtrate through the damaged BBB creating osmotic pressure difference between the capillary and interstitial space. This can cause the flux of water from the capillary and accumulate in the tissue space and causes the formation of vasogenic oedema, eventually leading to the formation of cerebral tissue swelling. Figure 2.1 illustrates the process of water accumulation into the interstitial space after BBB breakdown.

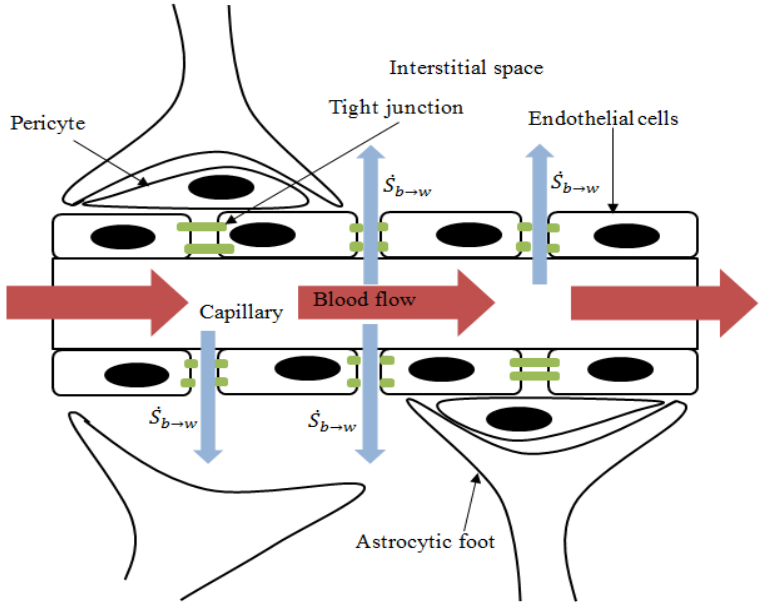

Figure 2.1: Flux of water after BBB breakdown. $\dot{S}_{b\to w}$ represents the water movement from the cerebral blood flow into the tissues via capillary filtration.

2.2.2. Poroelasticity Model: Mathematical Formulation

The formation of cerebral tissue swelling due to capillary filtration has been modelled by [4] using capillary filtration model and poroelastic theory. The governing equations are given as:

$$\sigma_{ij} - \alpha_w \nabla P_w = 0 \qquad (2.1)$$

$$\frac{1}{Q_w}\frac{\partial P_w}{\partial t} - k_w \nabla^2 P_w - \dot{S}_{b\to w} = 0 \qquad (2.2)$$

where σ_{ij} is the total stress of the tissue, P_w is the interstitial water pressure, α_w is the Biot parameter for water, Q_w is the relative compressibility of water, k_w is the permeability of water, t is time.

The term $\dot{S}_{b\to w}$ represents the water transfer from the capillary space into the cerebral interstitial space via capillary filtration, which occurs when BBB broke down. This term can be described by [4]:

$$\dot{S}_{b\to w} = 2\bar{n}_b \frac{L_p}{R_c} f[(P_b - P_w) - \sigma \Pi_b] \qquad (2.3)$$

where $\bar{n}_b$ is the baseline volume fraction of the blood, L_p is the hydraulic permeability of the capillary, R_c is the baseline value of capillary radius, σ is the reflection coefficient, Π_b is the osmotic pressure in the capillary and P_b is the blood pressure, which has been assumed constant. Lastly, the term f represents the fraction of vessels that remain open after the reperfusion and swelling process at each point in space and time, and this can be modelled using a Heaviside function.

The total stress, σ_{ij}, is linearly related to the strain, ε_{ij}, using typical linear elasticity relation:

$$\sigma_{ij} = 2G\varepsilon_{ij} + \frac{2Gv}{1-2v}\varepsilon_{ii} \qquad (2.4)$$

where G, and v are the shear modulus and Poisson's ratio of the brain tissue, respectively.

2.2.3. Numerical Procedure

2.2.3.1. Brain geometry and meshing

The brain geometry was drawn according to the realistic brain geometry as proposed by [16]. The brain is modelled as a circle that consists of a circular core in the middle that represents the brain ventricle. The brain radius is about 65 to 67 mm [17], hence the outer radius is taken here to be approximately as 80 mm. The circular core that represent the ventricle has the radius of 24 mm, taken to be about 30% of the brain radius [18]. The brain tissue is assumed to be homogeneous, thus there is no difference between the white and grey matter. The inner and outer boundaries of the brain geometry are named as the ventricular layer and the subarachnoid layer, respectively.

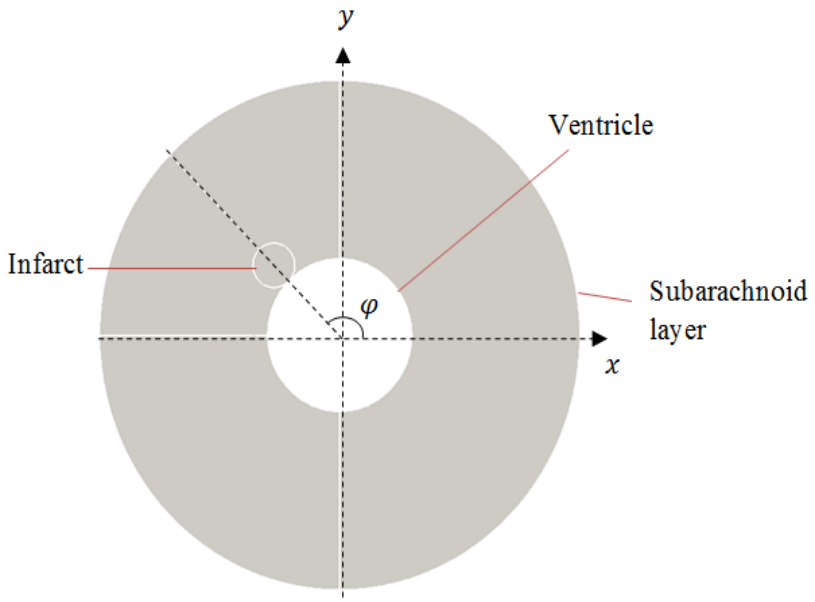

Figure 2.2: Idealized 2D brain geometry with an infarct of radius 7 mm located at $\boldsymbol{\varphi} = 135^{o}$.

To model the effects of ischaemia, a small infarcted region is drawn within the geometry. The infarct size is varied in the range 7 mm to 28 mm radius to study the effect of size on cerebral swelling. The infarct is drawn as a circle which is located along the line that makes an angle $\boldsymbol{\varphi} = 135^{o}$, where $\boldsymbol{\varphi}$ is the angle measured counterclockwise from the *x*-axis, as shown in Figure 2.2.

The infarcted region and region near it are discretised using a finer mesh than the rest of the part of the geometry. The number of elements varies depending on the sizes of the infarct of about 2000 to 5000 10-nodes tetradhedral elements. The meshing is done using Gmsh.

2.2.3.2. Boundary conditions

The boundary condition at the skull, R_s is set as stationary and pressure at baseline ICP, $\bar{P}$. The tissue is assumed to initially static and the fluid pressure is at the baseline ICP. Meanwhile, we consider two types of boundary conditions at the ventricle, R_V, which are: (1) the ventricle is assumed fix and the pressure is at the baseline ICP; and (2) the ventricle is free to move during tissue swelling:

$$\sigma_{ij}(R_V, t) \cdot \boldsymbol{n} = -\bar{P}\boldsymbol{n} \qquad (2.5)$$

The simulations are solved using open-source finite element analysis software ELMER and are analysed using ParaView.

2.2.3.3. Model parameters

Table 2.1 below shows the parameters involved in this model and their respective value. Details regarding the parameters can be found in [4].

2.3. Results and Discussion

2.3.1. Fix Ventricle Boundary Condition

The brain tissue swelling during capillary filtration was simulated for simulation time until 1 hour. Figure 2.3 shows the cerebral interstitial pressure P_w and tissue displacement u for various infarct sizes for the case of fix ventricle boundary condition. The tissue displacement starts to develop at the outermost radius of the infarct before slowly spreading to the inside and outside of the infarct. Meanwhile, the pressure starts to rise within the centre of the core and then spreads in the direction of the infarct radius.

Table 2.1: List of parameters and their baseline value for the proposed model.

Parameter	Value	Parameter	Value
v	0.35	P_b	4389 Pa
G	216.3 Pa	$\bar{n}_b$	0.03
α_w	1	L_p	3.0×10^{-11} m/s.Pa
Q_w	3244 Pa	R_c	5×10^{-6}m
Π_b	2445 Pa	$\bar{P}$	1330 Pa
σ	0.93		

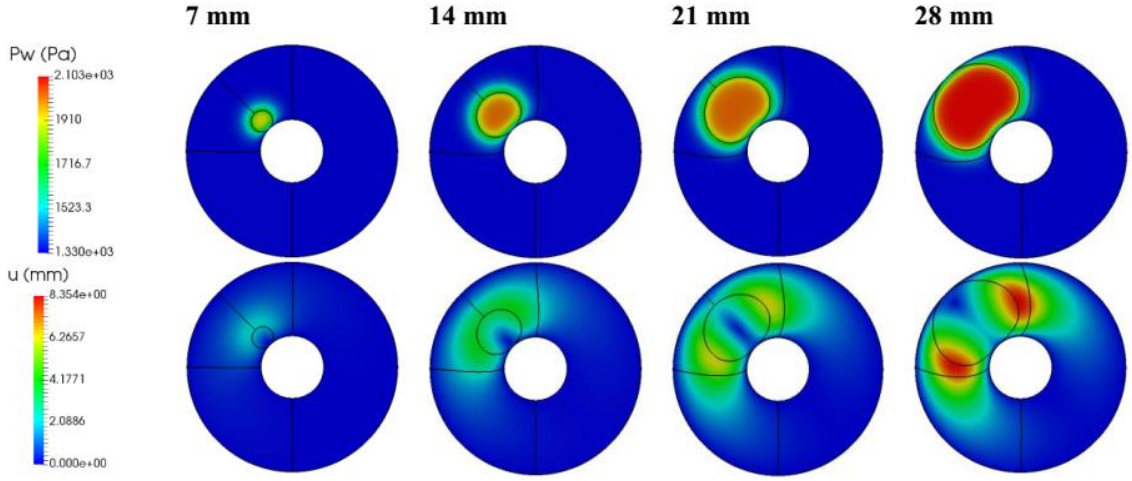

Figure 2.3: 2D simulation results for various infarct sizes. (Top) Interstitial pressure. (Bottom) Tissue displacement.

However, due to the boundary conditions imposed at the subarachnoid and ventricular layers, the displacement and pressure gradually decrease near these layers. The tissue displacement pushes the other side of the cerebral tissue as indicated by the deformation of the middle line to the right side. The deformation of this line increases as the size of the infarct becomes larger.

The changes in maximum displacement and maximum pressure when the infarct distance from the ventricle is varied are shown in Figure 2.4. The maximum displacement increases when the distance from the ventricle increases except for the case of the infarct radius at 7 mm. For this infarct size, there is a slight drop in the maximum displacement for the infarct distance from 7 mm to 21 mm and the infarct distance from 42 mm to 49 mm. Meanwhile, for the maximum pressure, there is no substantial difference when the

distance is varied with the exception of the case for a 7 mm infarct radius, although the difference for this case is only about 25 Pa from the other case.

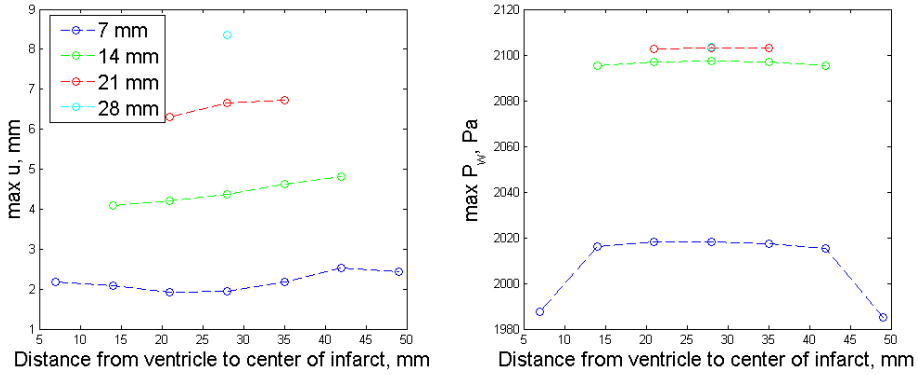

Figure 2.4: Variation of the maximum brain tissue displacement and interstitial pressure with the infarct size and distance from the ventricle.

This difference is due to the 'edge effect', in which the infarct is located near the subarachnoid and ventricle layer that have been fixed in terms of displacement and pressure values. In reality, the ventricle does not have a fixed shape and position but it may move and be compressed during brain tissue swelling. The compression of the ventricle is also a good indicator of cerebral swelling in CT images [19]. It is known that the existence of AQP4 at the interface of the ventricle and the cerebral space can help in the clearance of oedematous fluid [20]. Thus, a further improvement to the model could be made by incorporating a pressure gradient [21] and stress-free boundary conditions [22] at the ventricle to see how the presence of this fluid cavity affects the progression of cerebral swelling and fluid pressure development. However, for the sake of model simplification, this assumption is applied here.

2.3.2. Moving Ventricle Boundary Condition

For moving ventricle cases, we only consider two different sizes of stroke infarct – 7 mm and 14 mm radii. Then, we measure the displacement of two points on the ventricle, namely point x1 and x2 as illustrated in Figure 2.5.

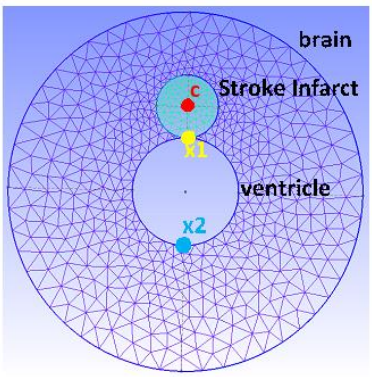

Figure 2.5: Location of x1 and x2 for ventricle displacement measurement.

Figure 2.6 shows the displacement of point x1 for stroke infarct of radius 7 mm and 14 mm at 7 and 5 different locations, respectively. The 0 mm and 42 mm lines referred to the stroke located nearest and farthest from the ventricle, respectively.

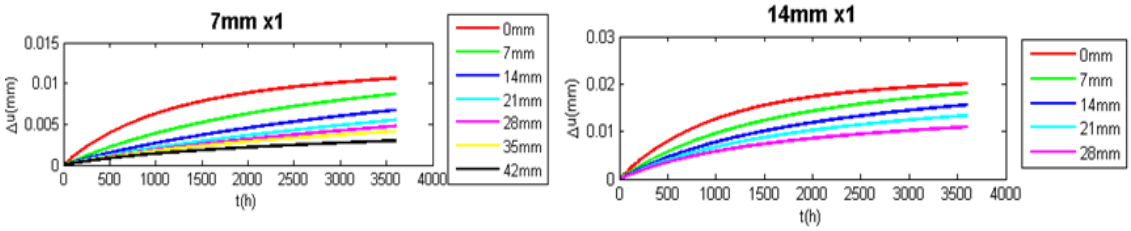

Figure 2.6: Displacement of point x1 for infarct radius of 7 mm and 14 mm.

It can be seen in Figure 2.6 that the displacement of point x1 increases as the simulation time increases for all locations of the stroke. Stroke that is located nearer to the ventricle results in larger displacement of point x1, whereas stroke located further shows smaller displacement. The changes in displacement for both 7 mm and 14 mm stroke shows similar characteristic, where the displacement increase rapidly from time 0 to 2000 s. After time 2000 s, the displacement becomes almost constant. However, the displacement of point x1 is bigger for 14 mm compared to 7 mm.

Meanwhile, Fig. 7 shows the displacement of point x2 for infarct radius of 7 mm and 14 mm. It can be seen here that the displacement of point x2 increases with time for all infarct locations, with exception for the case of infarct located 0 mm and 26 mm from the ventricle, for infarct radius of 7 mm and 14 mm, respectively. It should be noted that

the displacements of point x2 are much smaller compared to point x1 because point x2 is relatively farther from the stroke location than point x1.

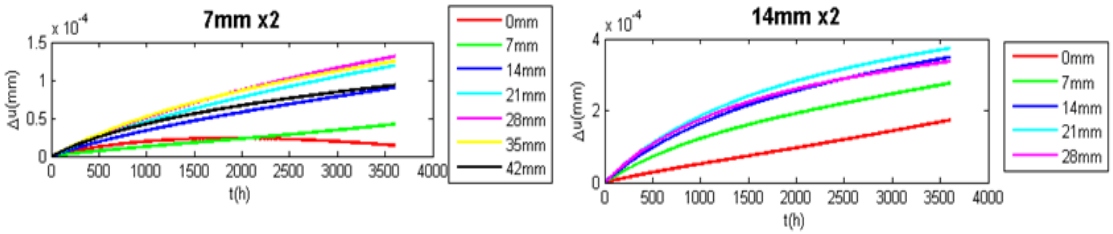

Figure 2.7: Displacement of point x2 for infarct radius of 7 mm and 14 mm.

Meanwhile, Figure 2.7 shows the displacement of point x2 for infarct radius of 7 mm and 14 mm. It can be seen here that the displacement of point x2 increases with time for all infarct locations, with exception for the case of infarct located 0 mm and 26 mm from the ventricle, for infarct radius of 7 mm and 14 mm, respectively. It should be noted that the displacements of point x2 are much smaller compared to point x1 because point x2 is relatively farther from the stroke location than point x1.

It is important to measure the displacement of the ventricle because brain swelling after stroke can be observed by looking at the movement of ventricle in MRI images. For example, ventricle enlargement has been used as an objective measure of mild cognitive impairment in Alzheimer's disease [23]. To further accurately measure ventricle movement will require the integration of the finite element model with brain images through image-model registration procedure, as has been done, for example, by [24].

2.4. Future Works

It has been assumed in this study that the cerebral tissue property is homogeneous throughout the geometry. In reality, the cerebral tissue material properties are different for those located in the white and grey matter of the cerebral space. Oedema is less likely to develop in the grey matter area due to its twisted structure and it has a low tissue

compliance as compared to white matter [25]. The study done by Smillie, et al. [18] also assumed that the mechanical properties of white and grey matter are the same due to the lack of data available. However, they use different fluid permeability values within these two cerebral structures. Meanwhile, the model developed by Nagashima, et al. [26] used two different cerebral tissue hydraulic conductivity values to account for their different properties. Therefore, incorporating the different mechanical properties of the brain tissues in the model could improve the brain tissue swelling prediction.

Another aspect worth studying is the vasogenic oedema resolution. The oedematous fluid will move out into the ventricles and subarachnoid spaces via glia limitans, into the capillary endothelium via the astrocytic foot or by metabolic degradation [27, 28]. The presence of aquaporin-4 (AQP4) channels in the glia limitans and astrocytic foot [28] facilitate the removal of the oedematous fluid. However, AQP4 also plays a role in the formation of cytotoxic oedema that causes intracellular swelling, which does not result in an increase in ICP and brain tissue swelling [29]. The function of AQP4 has been demonstrated by using a mathematical model [30]. Modification of the current model through the inclusion of the role of AQP4 might provide new insight towards the occurrence of reperfusion injury.

2.5. Conclusion

From this study, it was found that the size and location of cerebral ischaemic infarct can affect the degree of brain herniation. This is shown by the deflection of the midline that divides the two cerebrals. In addition, the maximum brain tissue displacement and interstitial pressure are increase as the infarct sizes increase. These findings indicate that ischaemic infarct size plays an important role in determining the severity of brain tissue swelling.

The results obtained here provide further useful information such as: (1) the importance of making the ventricle structure movable for better quantification of the brain tissue swelling; and (2) confirms the occurrence of herniation during brain tissue swelling. This information is useful before the models can be applied to the actual patient data for validation purposes.

Chapter 3: Application of asymptotic expansion homogenization for vascularized poroelastic brain tissue

3.1. Introduction

Poroelastic theory has been used to derive a mathematical model to describe brain tissue swelling due to oedema after an ischaemia-reperfusion injury [4]. This model has also been used to investigate the function of aquaporin-4 (AQP4) in the formation and elimination of brain oedema [30]. This model has been shown to provide potential to be used as a tool to predict suitable reperfusion treatment conditions to prevent brain oedema formation. In this model, however, the blood pressure is assumed homogeneous throughout the brain as well as the blood capillaries are assumed to have similar sizes, which considerably simplify the model. However, in the brain, it has been proven experimentally that the blood capillaries diameters are normally distributed with a mean of 6.23±1.3 μm [31].

Asymptotic expansion homogenization (AEH) has been used in the Darcy's and Navier-Stokes models to derive a new set of homogenized governing equations and associated microscale cell problems [32]. This method is then applied by [33] on a cerebral capillary network generated by fitting the experimental data of [31] using Modified Spanning Tree Method (MSTM) [34]. They obtained the interstitial fluid permeability tensor, which is isotropic. The same method also has been used by [35] on an ideal capillary network to investigate the importance of capillary tortuosity in tumor. However, these applications did not take tissue displacement into account, which will make the model to be able to predict tissue movement and is important for the application of brain tissue swelling prediction.

Darcy's law is strongly related with the poroelastic theory by the inclusion of Biot's coefficient [11]. Hence, applying the AEH technique on poroelastic theory could enable the determination of tissue displacement as an effect of fluid transport in between the capillary and the interstitial. Application of AEH technique on vascularized poroelastic material has been done by [36] but more towards theoretical derivations. In this paper, water transport between the capillary and the interstitial fluid of brain tissue will be modelled using poroelastic theory and Navier-Stokes equation, and AEH technique will be applied to obtain a new set of homogenized macroscale governing equations and their associated microscale cell problems. The microscale cell problems are required to be solved first before the macroscale governing equations can be solved on a larger brain geometry. An example of solving the microscale cell problems on an ideal brain tissue with embedded capillary geometry will be shown in this paper.

3.2. Methodology

3.2.1. Governing equations

Consider a vascularized brain tissue $\Omega = \Omega_t \cup \Omega_c$ where Ω_t and Ω_c are the poroelastic brain tissue (which consists of interstitial fluid and solid matrix) and capillary network compartments, respectively. We assumed that the intercapillary distance d is much smaller than the average brain size L such that:

$$\epsilon = \frac{d}{L} \ll 1 \qquad (3.1)$$

in which we can then define two independent spatial variables x and y representing the macro- and micro-scale, respectively, such that:

$$\epsilon = \frac{x}{y} \qquad (3.2)$$

and

$$\nabla \rightarrow \nabla_x + \frac{1}{\epsilon}\nabla_y \quad (3.3)$$

In addition, we define $\Gamma = \partial\Omega_t \cap \partial\Omega_c$ as the interface between the two compartments.

In the poroelastic compartment, the stress equilibrium is given as:

$$\nabla \cdot \sigma_t = 0 \; in \; \Omega_t \quad (3.4)$$

neglecting external body forces. Here, the stress tensor σ_t is related with the solid matrix displacement u and the interstitial pressure P_t such that:

$$\sigma_t = \mathbb{C}: \nabla u - \alpha P_t I \quad (3.5)$$

where α is the Biot coefficient and $\mathbb{C}$ is the stiffness tensor of the solid matrix, which is is defined as:

$$\mathbb{C} = \mathbb{C}(E, v) \quad (3.6)$$

Here, E and v are the Young's modulus and Poisson's ratio of the solid matrix.

The interstitial pressure P_t can then be related to the interstitial fluid velocity v_t by Darcy's law:

$$w_t = \frac{k}{\mu}\nabla P_t \; in \; \Omega_t \quad (3.7)$$

where k and μ are the permeability of the poroelastic medium and fluid viscosity, respectively, and w_t is the relative interstitial velocity such that:

$$w_t = \phi(v_t - \dot{u}) \quad (3.8)$$

Here, ϕ is the porosity of the medium. Using mass conservation for the poroelastic compartments to get:

$$\dot{P}_t = -\alpha M \nabla \cdot \dot{u} - M \nabla \cdot w_t \; in \; \Omega_t \quad (3.9)$$

where M is the relative compressibility of the interstitial fluid.

Meanwhile, in the capillary network, the blood is assumed as an incompressible Newtonian fluid and the Navier-Stokes' law holds:

$$\nabla \cdot \sigma_c = 0 \; in \; \Omega_c \qquad (3.10)$$

$$\nabla \cdot v_c = 0 \; in \; \Omega_c \qquad (3.11)$$

where σ_c is the blood network stress tensor:

$$\sigma_c = -P_c I + \mu_c(\nabla v_c + (\nabla v_c)^T) \qquad (3.12)$$

Assuming continuity of stresses on Γ between the two compartments, we get:

$$\sigma_c \boldsymbol{n} = \sigma_t \boldsymbol{n} \; on \; \Gamma \qquad (3.13)$$

where n is the unit vector normal to the Γ surface. The normal component of the velocities at Γ follow the relationship below:

$$(v_c - \dot{u}) \cdot \boldsymbol{n} = \left((\alpha - 1)\dot{u} + w_t\right) \cdot \boldsymbol{n} \; on \; \Gamma \qquad (3.14)$$

The fluid transport across Γ between the capillary network and poroelastic compartments is required, to model, for example, water transport across blood-brain barrier (BBB) into brain tissue interstitial during ischaemia-reperfusion [4]. This can be described as:

$$(v_c - \dot{u}) \cdot \boldsymbol{n} = -\epsilon L_p(\boldsymbol{n}(\sigma_c \cdot \boldsymbol{n}) + P_t) \; on \; \Gamma \qquad (3.15)$$

where ϵL_p measures the amount of fluid leaks from the capillary into the interstitial space.

In addition, we also consider the fluid slip over the porous surface, which can be modelled using the Beavers-JosephSaffman conditions as:

$$\boldsymbol{t} \cdot (\sigma_c \boldsymbol{n}) = -\frac{\beta \mu_c}{\sqrt{k}} (v_c - \dot{u}) \cdot \boldsymbol{t} \; on \; \Gamma \qquad (3.16)$$

where $\boldsymbol{t}$ is the tangential direction to Γ and β is the Beavers-Joseph parameter.

3.2.2. Asymptotic Expansion Homogenization Technique

Equations (4) to (16) will first be non-dimensionalized before the asymptotic expansion homogenization (AEH) technique is applied. AEH is used to derive a new set of homogenized marcroscale governing equations for the PDE systems (3.3) to (3.15). The PDE variables P_t, P_c, w_t, v_c, u, σ_t, and σ_c are assumed to be functions in terms of x

and y. Employing power series expansion for every variables (collectively denoted as F) to get:

$$F(x,y,t) = \sum_{l=0}^{\infty} F^{(l)}(x,y,t)\epsilon^l \quad (3.17)$$

It is assumed that all of the PDE variables is periodic with respect to y.

We also define the cell average operator such that:

$$\langle(.)\rangle = \frac{1}{|\Omega|}\int_{\Omega_a}(.)\,dy \quad (3.18)$$

where $|\Omega|$ is the total volume of the microscale periodic cell and $a = t, c$. It should be noted that the volume fraction of a-portion of the cell is given by:

$$\phi_a = \frac{|\Omega_a|}{|\Omega|}, a = t, c \quad (3.19)$$

Using (17) and (3) on each variable in (4) to (16), the power series expansions for each of the variables P_t, P_c, w_t, v_c, u, σ_t, and σ_c are obtained and the power for $\epsilon^{(l)} = 0,1,$ ... are compared. Through these processes, it is found that the variables $P_t^{(0)}$, $P_c^{(0)}$ and $u^{(0)}$ are y-constant, that is:

$$P_t^{(0)} = P_t^{(0)}(x,t) \quad (3.20)$$

$$P_c^{(0)} = P_c^{(0)}(x,t) \quad (3.21)$$

$$u^{(0)} = u^{(0)}(x,t) \quad (3.22)$$

3.2.3. Microscale Cell Problems and Homogenized Macroscale Governing Equations

Through the AEH technique, the macroscale homogenized governing equations in the homgenized domain are obtained as below:

$$\nabla_x \cdot \sigma_H = 0 \quad (3.23)$$

$$\sigma_H = (\mathbb{C}L\mathbb{C} + \mathbb{C}) : \nabla_x u^{(0)} + (\mathbb{C} : Q - \phi_c I)P_c^{(0)} - \alpha(\mathbb{C} : Q + \phi_t I)P_t^{(0)} \quad (3.24)$$

$$\frac{\dot{P}_c^{(0)}}{M_H} = -\nabla_x \cdot \langle w_c^{(0)}\rangle_c - (\phi_c I - \mathbb{C} : Q) : \nabla_x \dot{u}^{(0)} + \frac{\alpha}{M_H}\dot{p}_t^{(0)} - \frac{|\Gamma|L_p}{|\Omega|}\left(P_c^{(0)} - P_t^{(0)}\right) \quad (3.25)$$

$$\dot{P}_t^{(0)}\left(\frac{\phi_c}{M}+\frac{\alpha}{M_H}\right)=-\nabla_x\cdot\langle w_t^{(0)}\rangle_t-(\alpha\phi_c I-\mathbb{C}:Q):\nabla_x\dot{u}^{(0)}+\frac{\dot{p}_c^{(0)}}{M_H}-\frac{|\Gamma|L_p}{|\Omega|}\left(P_c^{(0)}-P_t^{(0)}\right) \quad (3.26)$$

$$\langle w_c^{(0)}\rangle_c=-K\nabla_x P_c^{(0)} \quad (3.27)$$

$$\langle w_t^{(0)}\rangle_t=-kG\nabla_x P_t^{(0)}-(\alpha-1)(\nabla_y P_t)\dot{u}^{(0)} \quad (3.28)$$

where the $w_t^{(0)}$ and $w_c^{(0)}$ are the leading order interstitial fluid and blood velocities, and M_H is given by:

$$M_H=-\frac{1}{tr(Q)} \quad (3.29)$$

The tensors L, Q, K, and G can be obtained by solving the following four cell problems on a cell geometry independently:

Laplace cell problem:

$$\nabla_y^2 P_t=0\ in\ \Omega_t \quad (3.30)$$

$$\nabla_y P_t\cdot\boldsymbol{n}=\boldsymbol{n}\ on\ \Gamma \quad (3.31)$$

$$\langle P_t\rangle_t=0 \quad (3.32)$$

$$G=\phi_t I-\langle\nabla_y P_t\rangle_t \quad (3.33)$$

Stokes' cell problem:

$$\nabla_y P_c=\nabla_y^2 W^T+I\ in\ \Omega_c \quad (3.34)$$

$$\nabla_y\cdot W^T=0\ in\ \Omega_c \quad (3.35)$$

$$W^T=0\ on\ \Gamma \quad (3.36)$$

$$\langle P_c\rangle_c=0 \quad (3.37)$$

$$K=\langle W\rangle_c \quad (3.38)$$

One-elastic cell problem:

$$\nabla_y\cdot\left(\mathbb{C}:\nabla_y a\right)=0\ in\ \Omega_t \quad (3.39)$$

$$\left(\mathbb{C}:\nabla_y a\right)\boldsymbol{n}=-\boldsymbol{n}\ on\ \Gamma \quad (3.40)$$

$$\langle a\rangle_t=0 \quad (3.41)$$

$$Q=\langle\nabla_y a\rangle_t \quad (3.42)$$

6-elastic cell problem:

$$\nabla_y \cdot \left(\mathbb{C} : \nabla_y A\right) = 0 \; in \; \Omega_t \qquad (3.43)$$

$$\left(\mathbb{C} : \nabla_y A\right)\boldsymbol{n} = -\boldsymbol{n} \; on \; \Gamma \qquad (3.44)$$

$$\langle A \rangle_t = 0 \qquad (3.45)$$

$$L = \langle \nabla_y A \rangle_t \qquad (3.46)$$

Here, P_t, P_c, and a are auxiliary vectors, W is auxiliary second order tensor, and A is auxiliary third order tensor. It should be noted here that G, K, and Q are second order tensors, while L is a fourth order tensor.

These cell problems must be solved first on a cell geometry before the homogenized macroscale governing equations can be solved on a bigger brain geometry. In the next subsection, an example of solving these cell problems on a simple cubic cell geometry is shown.

3.2.4. Solving Microscale Cell Problems

A cubic cell geometry representing brain tissue is as shown in the Figure 3.1. To model the capillary embedded in the tissue, a simple 6-branch cylinders are drawn representing the capillary. In addition, the brain tissue mechanical properties are assumed to be linear elastic and have stiffness tensor $\mathbb{C} = \mathbb{C}(584\ Pa, 0.35)$. Table 3.1 shows the brain tissue geometrical and mechanical properties.

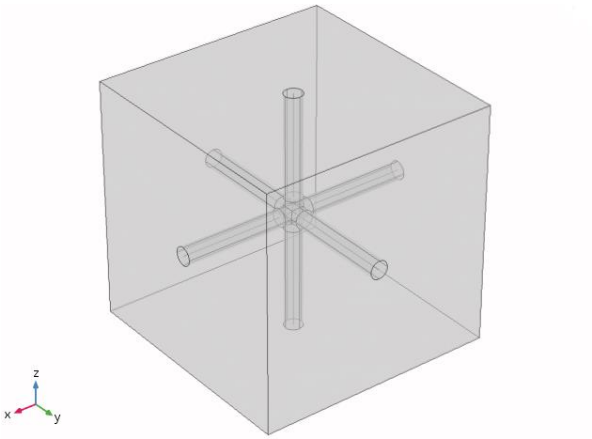

Figure 3.1: Brain tissue represented by a cubic cell geometry.

Table 3.1: Brain tissue geometrical and mechanical properties.

Parameter	Description	Value
l	Brain tissue length	1.84
l_c	Capillary branch length	0.84
h	Capillary cylindrical link	0.24
Ω	Brain tissue volume	6.23
d	Microscale length	40 μm
L	Macroscale length	1 cm

Each of the cell problem will be solved one by one using COMSOL multiphysics standard PDE solvers. Standard P2-P1 discretization is used for the Stokes' cell problem, whereas for the other cell problems, a standard quadratic-Lagrange discretization is used.

3.3. Results

3.3.1. Laplace Cell Problem

Solving Laplace cell problem (3.30) to (3.33) to obtain the tensor G, which in componentwise form is:

$$G_{ij} = \phi_t \delta_{ij} - \langle \frac{\partial P_{t_i}}{\partial y_j} \rangle_t$$

Solving for x-, y-, and z-components to obtain G_{1j}, G_{2j}, and G_{3j}, respectively. Figure 3.2 shows the distribution of P_{t_1} solved on the poroelastic compartment.

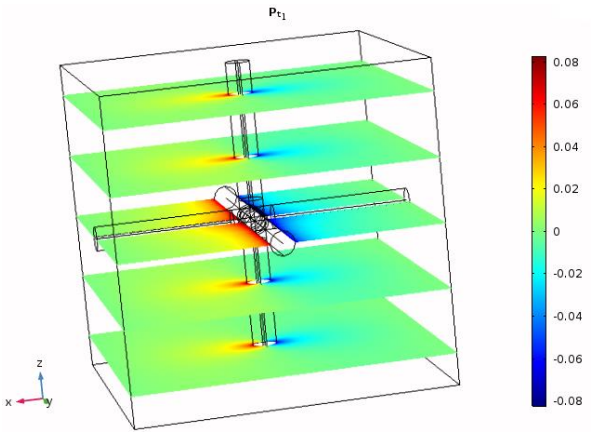

Figure 3.2: Distribution of P_{t_1}.

G is calculated as:

$$G_{ij} = \begin{pmatrix} 0.9781 & 0 & 0 \\ 0 & 0.9781 & 0 \\ 0 & 0 & 0.9781 \end{pmatrix} \approx 0.98I$$

taking the non-diagonal elements as zero because it is much smaller than the diagonal elements.

3.3.2. Stokes' Cell Problem

Stokes' cell problem is solved to obtain the tensor K, which can be obtained by solving (3.38) componentwise such that:

$$K_{ij} = \langle W_{ij} \rangle_c$$

Solving (3.34) to (3.37) in x-, y-, and z-components to obtain W_{1j}, W_{2j}, and W_{3j}, respectively. Figure 3.3 below shows the distribution of W_{1j} obtained in the capillary compartment when solving the Stokes' cell problem (3.34) to (3.37) in x-component.

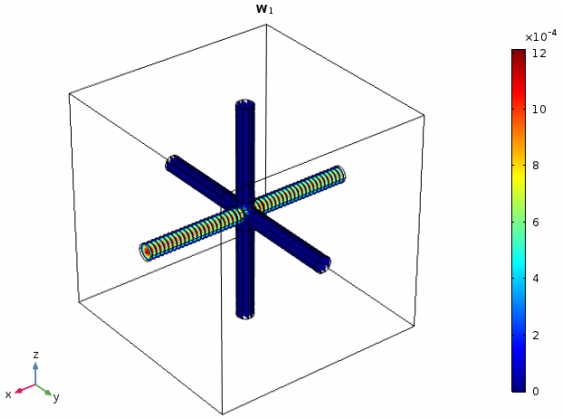

Figure 3.3: Distribution of W_{1j}.

K is calculated as:

$$K_{ij} = \begin{pmatrix} 2.6296 \times 10^{-6} & 0 & 0 \\ 0 & 2.6292 \times 10^{-6} & 0 \\ 0 & 0 & 2.6292 \times 10^{-6} \end{pmatrix} \approx 2.63 \times 10^{-6} I$$

where the non-diagonal values of K are much smaller than its diagonal values.

3.3.3. One-Elastic Cell Problem

Equations (3.39) to (3.41) are solved to obtain the tensor Q, which can be described in componentwise form as:

$$G_{ij} = \langle \frac{\partial a_i}{\partial y_j} \rangle_t.$$

Solving the cell problem in x-, y-, and z-components to obtain a_1, a_2, and a_3, respectively. Figure 3.4 shows the distribution of a_1.

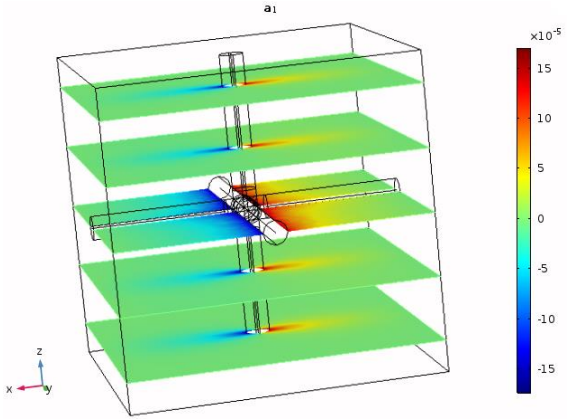

Figure 3.4: Distribution of a_1.

Q is calculated as:

$$Q_{ij} = \begin{pmatrix} 1.8199 \times 10^{-5} & 0 & 0 \\ 0 & 1.8195 \times 10^{-5} & 0 \\ 0 & 0 & 1.8199 \times 10^{-5} \end{pmatrix} \approx 1.82 \times 10^{-5} I$$

with the non-diagonal values are approximately zero. Q can then be used to calculate M_H:

$$M_H = -18315$$

and also to calculate $\mathbb{C}$: Q:

$$\mathbb{C}: Q = 17.07 \times 10^{-3}.$$

3.3.4. 6-Elastic Cell Problem

Solving the 6-elastic cell problem (3.43) to (3.46) to get the fourth order tensor L, which has the following componentwise form:

$L_{ijkl} = \langle \frac{\partial A_{ikl}}{\partial y_j} \rangle_t$.

The tensor L can be obtained by solving for $k > l; k, l = 1,2,3$ for x-, y-, and z-components. Figure 3.5 shows the solutions for the cell problem for different i, j, k, l combinations. The tensor L can be rewritten in second order form using Voigt notation.

Then, the following tensor can be calculated:

$$(\mathbb{C}L\mathbb{C} + \mathbb{C}) = \begin{pmatrix} 964.9 & 527.4 & 527.4 & & & \\ 527.4 & 964.9 & 527.4 & & 0 & \\ 527.4 & 527.4 & 964.9 & & & \\ & & & 219.7 & 0 & 0 \\ & 0 & & 0 & 219.7 & 0 \\ & & & 0 & 0 & 219.7 \end{pmatrix}$$

which is isotropy because $\mathbb{C}$ elements being very large compared to L.

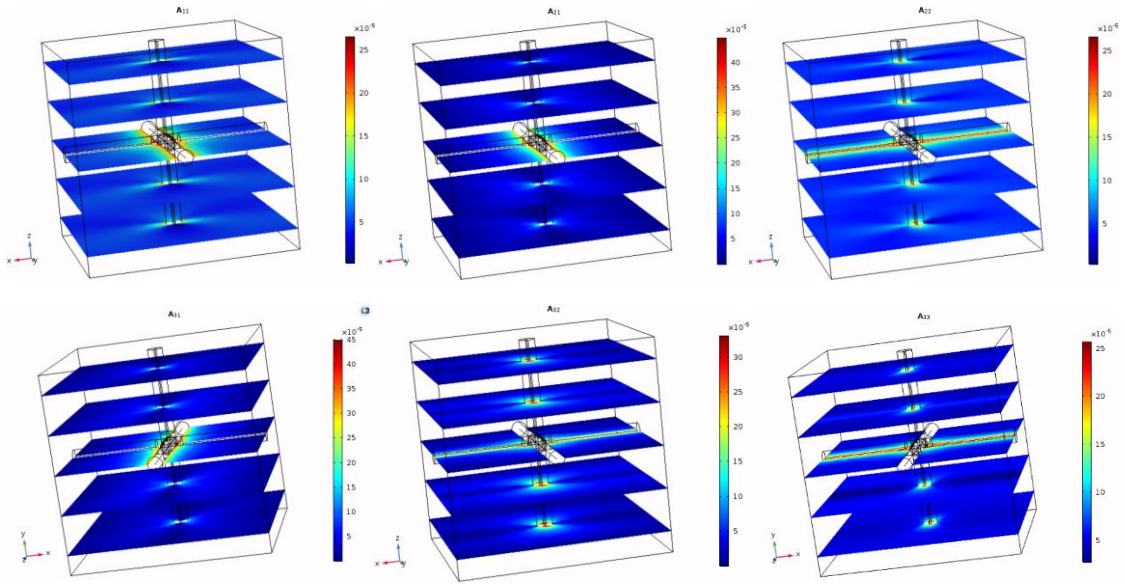

Figure 3.5: From left to right. Top: Distribution of A_{11}, A_{21}, and A_{22}. Bottom: Distribution of A_{31}, A_{32}, and A_{33}.

3.4. Discussion

Solving the microscale cell problems (3.30) to (3.46) are essential to obtain the tensors L, Q, K, and G before they can be used to solve the homogenized macroscale governing equations (3.23) to (3.28). The microscale cell problems must be solved in a brain tissue

geometry. In this paper, an ideal cubic brain tissue embedded with 6-branch cylindrical capillaries is used as the geometry where the microscale cell problems are solved. In the future, the capillary can be made twisted and kinked to simulate the effect of capillary tortuosity as has been done by [35]. Further, the brain capillary distribution can also be considered by using the statistically accurate brain capillary network created in [34] to allow for a more accurate modelling of the brain oedema formation problem.

The tensors L, Q, K, and G if compared with the poroelastic model used by [4] have their own physical meanings. For examples, K and G are analogous to the interstitial fluid and blood permeability in the porous tissue, respectively. Meanwhile, the tensors L and Q are important in determining the analogous effective stiffness tensor and Biot coefficient, respectively. These four tensors depend greatly on the brain tissue compositions at microscale level. In this paper, the tensors Q, K, and G are isotropy, while L is not, however, its effect on the effective stiffness tensor is not significant enough to make it not isotropic. Further investigation using a more complex capillary configuration is needed to see the properties of these tensors and their effects on the macroscale governing equations.

3.5. Conclusion

The AEH technique has been applied on the vascularized poroelastic model for the application of brain oedema formation in the brain tissue. Microscale cell problems are obtained and have been solved on an ideal brain tissue geometry with blood capillary embedded inside. The tensors L, Q, K, and G are calculated as an example and their values are greatly affected by the capillary distribution in the brain tissue geometry, which will be the subject of a future work.

Chapter 4: Effects of brain tissue mechanical and fluid transport properties during ischaemic brain oedema a poroelastic finite element analysis

4.1. Introduction

Brain herniation occurs when a part of the brain within the skull is being pushed as a result of an increase in the intracranial pressure (ICP). This phenomenon can be observed under the MRI and CT scans by the movement of the midline structures, particularly the brain ventricles. Brain herniation is usually used as an indicator of the occurrence of brain oedema or brain tissue swelling. Brain oedema formation has been observed in ischaemic stroke patients that received reperfusion treatments such as using mechanical catheterisation or by recombinant tissue plasminogen activator (rtpa) administration. Herniation is undesirable because it may lead to the compression of brain microvessels, resulting in secondary ischaemic stroke [9].

Current ischaemic stroke treatments must be given within a short time windows of up to 4.5 hours (if using rtpa), whereby treatments given after this time may increase the risk of ischaemia-reperfusion injury such as brain oedema [37]. However, most patients usually arrived late to the hospital due to many circumstances such as heavy traffic and late detection of stroke occurrence. Therefore, predicting the progression of brain oedema will greatly help neurosurgeon in determining the suitability of an ischaemic stroke treatment to prevent the occurrence of brain herniation, especially for patients that arrived late for the treatments.

A mathematical model describing the formation of brain tissue swelling after ischaemia-reperfusion treatment has been previously developed [4, 38, 39] using

poroelastic theory. This theory is initially developed to investigate soil consolidation phenomena [11], but has been extensively used to model fluid transport in biological tissue. The brain tissue is assumed to contain water and blood permeable in a porous solid matrix structure. The solid matrix is further assumed as linear elastic, homogeneous, and isotropic. In addition, the water and blood permeability and viscosity are also assumed to be isotropic and homogeneous. These assumptions were made for the sake of simplification of the model, while in fact the mechanical and fluid transport properties in the brain may be different from one patient to another.

In this chapter, the mathematical model developed will be solved in a realistic brain geometry using finite element scheme of poroelastic model. Then, the effect of varying the brain tissue Young's modulus, Poisson's ratio, water permeability, and viscosity will be investigated. This results will be used as a preliminary study to determine the importance of these parameters towards predicting brain oedema formation and also for estimating suitable parameters value. Currently, the value of these parameters were taken from related literature. However, each patient should have different parameters value which require estimation and optimization.

4.2. Methodology

4.2.1. Brain Oedema Formation by Capillary Filtration Model

Brain tissue region affected by ischaemia will experience lack of oxygen and nutrient due to blood flow reduction. This will initiate a series of biochemical reactions that destroys the endothelial cells lining the cerebral microvessels, resulting to the blood-brain barrier (BBB) breakdown. Upon reperfusion and blood flow has been restored, ions and some protein plasma can filtrate through the damaged BBB consequently creating osmotic pressure difference between the capillary and the interstitial space. The osmotic pressure

difference can cause water flux from the microvessels into the tissue space and the accumulation of water is known as brain oedema, eventually causing brain tissue swelling.

The formation of brain oedema can be modelled using capillary filtration model given by (4.1):

$$\dot{S}_{b\to w} = 2\bar{n}_b \frac{L_p}{R_c} f[(P_b - P_w) - \sigma \Pi_b] \qquad (4.1)$$

Here, the term $\bar{n}_b$ is the baseline volume fraction of the blood, L_p is the hydraulic permeability of the capillary, R_c is the baseline value of capillary radius, σ is the reflection coefficient, Π_b is the osmotic pressure in the capillary and P_b is the blood pressure, which has been assumed constant. Lastly, the term *f* represents the fraction of vessels that remain open after the reperfusion and swelling process at each point in space and time, and this can be modelled using a Heaviside function.

4.2.2. Poroelastic Model Formulation

The brain oedema will result in brain tissue movement or swelling. Poroelastic model is used to model brain tissue swelling during brain oedema. The governing equations for the poroelastic model are made up of stress equation as in (4.2) and pressure equation as in (4.3):

$$\sigma_{ij} - \alpha_w \nabla P_w = 0 \qquad (4.2)$$

$$\frac{1}{Q_w}\frac{\partial P_w}{\partial t} - k_w \nabla^2 P_w - \dot{S}_{b\to w} = 0 \qquad (4.3)$$

where σ_{ij} is the total stress of the tissue, P_w is the interstitial water pressure, α_w is the Biot parameter for water, Q_w is the relative compressibility of water, k_w is the permeability of water, and t is time. The term k_w can be related to the water specific permeability κ_w and viscosity μ_w by (4.4):

$$k_w = \frac{\kappa_w}{\mu_w} \tag{4.4}$$

The total stress, σ_{ij}, is linearly related to the strain, ε_{ij}, using typical linear elasticity relationship (4.5):

$$\sigma_{ij} = 2G\varepsilon_{ij} + \frac{2Gv}{1-2v}\varepsilon_{ii} \tag{4.5}$$

where G and v are the shear modulus and Poisson's ratio of the brain tissue, respectively. The strain ε_{ij} is related to the brain tissue displacement, u by (4.6):

$$\varepsilon_{ij} = \frac{1}{2}\left(\nabla u_i + \nabla u_j\right) \tag{4.6}$$

Lastly, the term Q_w is related to G and v by (4.7):

$$\frac{1}{Q_w} = \frac{\alpha_w - n_w}{K_S} + \frac{n_w}{K_w} \tag{4.7}$$

where K_S and K_w are the bulk moduli for the solid and fluid phases, respectively. Table 4.1 shows the model parameters and their respective reference value [4].

Table 4.1: Model Parameters.

Parameter	Value	Parameter	Value
v	0.35	μ_w	1.0×10^{-3} Pa.s
G	216.3 Pa	σ	0.93
α_w	1	P_b	4389 Pa
K_w	2.2×10^{9} Pa	L_p	3.0×10^{-11} m/s.Pa
n_w	0.8	R_c	5×10^{-6} m
Π_b	2445 Pa	$\bar{P}$	1330 Pa
κ_w	3.6×10^{-15} m^2		

4.2.3. Brain Geometry and Meshing

The brain geometry is as shown in Figure 4.1. The brain and ventricle geometry are developed from a typical structural T2 MRI of normal human. Meanwhile, the infarct geometry is created artificially by assuming the infarct to have a radius between 7 to 14 mm.

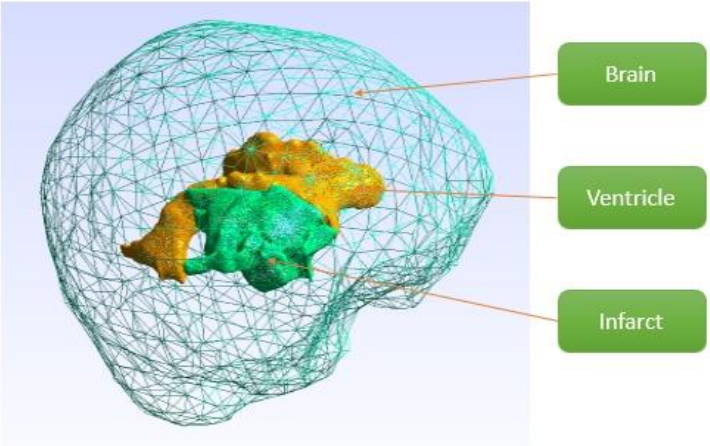

Figure 4.1: The model is solved in this brain geometry.

The ventricle surface and the infarct are finely meshed, while the brain is coarsely meshed, using tetrahedral elements. The total number of mesh is approximately 900,000. The geometry is meshed using open-source meshing software, Gmsh.

4.2.4. Finite Element Procedure

The outer boundary of the brain is set such that it is fixed to the rigid skull. Therefore, the boundary condition at the skull, R_S is set such that:

$$u(R_S, t) = 0 \tag{4.8}$$

$$P_w(R_S, t) = 1330\ Pa \tag{4.9}$$

To allow for brain ventricle movement as a result of brain tissue swelling for the purpose of mimicking brain herniation, the boundary condition on the surface of the ventricle, R_V is set such that:

$$\sigma_{ij}(R_V, t) \cdot \boldsymbol{n} = -\bar{P}\boldsymbol{n} \tag{4.10}$$

The simulations are solved using open-source finite element analysis software ELMER by coupling both diffusion equation and linear elastic solvers to solve for pressure equation and stress equation, respectively. Then, the results are analysed using ParaView.

4.3. Results

The simulation is performed to observe the swelling effect after 5 hours. Figure 4.2 shows the cerebral interstitial pressure and tissue displacement for a slice located approximately 15 mm from the top of the brain. From the figures, the tissue displacement starts to develop from the outermost radius of the infarct before it slowly spreads towards the inside and outside of the infarct. Meanwhile, the pressure starts to rise within the center of the infarct and then spreads in the direction of the infarct radius.

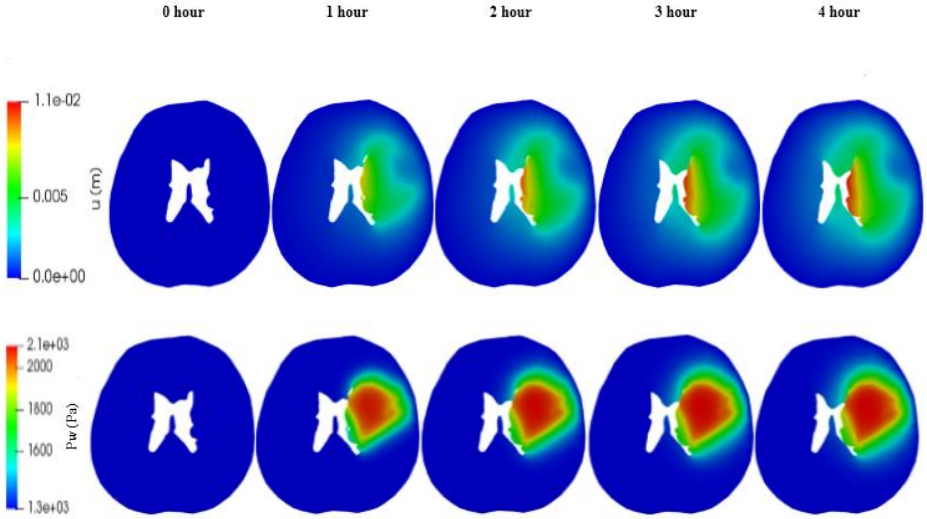

Figure 4.2: Brain tissue displacement (top) and interstitial pressure (bottom) distributions for a brain slice 15 mm from the top.

4.3.1. Effect of Varying Brain Tissue Young's Modulus and Poisson's Ratio

The reference value for the brain tissue Young's modulus and Poisson's ratio are 584 Pa and 0.35, respectively. These parameters are then varied within the range of 1000 to 4000 Pa and 0.2 to 0.4, respectively. These values are within the acceptable range of human brain tissue mechanical properties [4].

Figure 4.3 shows the maximum displacements taken at time 5 hours for different Young's modulus values. The change of displacement with time is initially similar for all Young's modulus, but reaching maximum at different displacement values. Largest

Young's modulus value (4000 Pa) results in the smallest brain tissue displacement of about 0.0015 mm, which roughly 87% smaller than the brain tissue displacement at reference Young's modulus value (584 Pa).

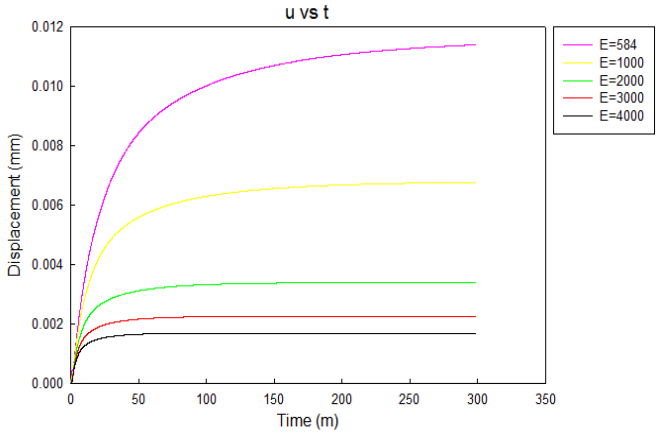

Figure 4.3: Brain tissue displacement for different brain tissue Young's modulus E.

The change of interstitial pressure when varying the brain tissue Young's modulus is as shown in Figure 4.4. All Young's modulus reaches similar maximum pressure at 2100 Pa although the time taken to reach the maximum are different. Smaller Young's modulus requires longer time to reach maximum pressure.

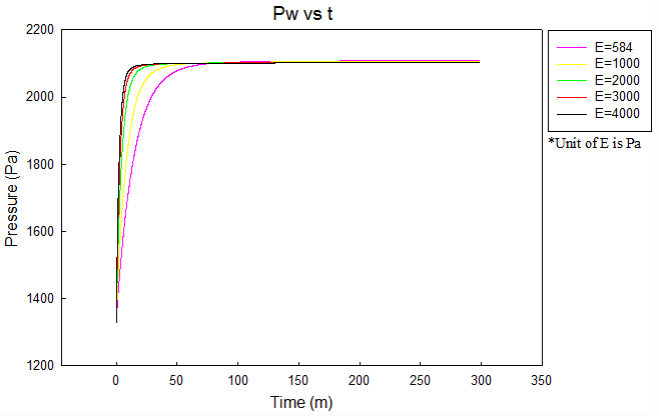

Figure 4.4: Brain tissue interstitial pressure for different brain tissue Young's modulus E.

Figure 4.5 shows the variation of maximum displacements for different brain tissue Poisson's ratio. The displacement varies linearly with time up until about 25

minutes but reaching different maximum displacement values. Smallest Poisson's ratio ($v = 0.2$) results in the highest displacement.

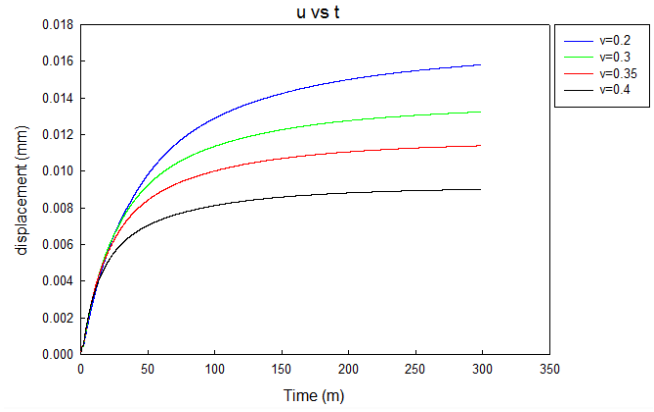

Figure 4.5: Brain tissue displacement for different brain tissue Poisson's ratio v.

Meanwhile, the variation of brain interstitial pressure for different Poisson's ratio values is as shown in Figure 4.6. The pressure reaches similar maximum value of 2100 Pa. for all values of v, but smaller v requires longer time for the pressure to reach the maximum.

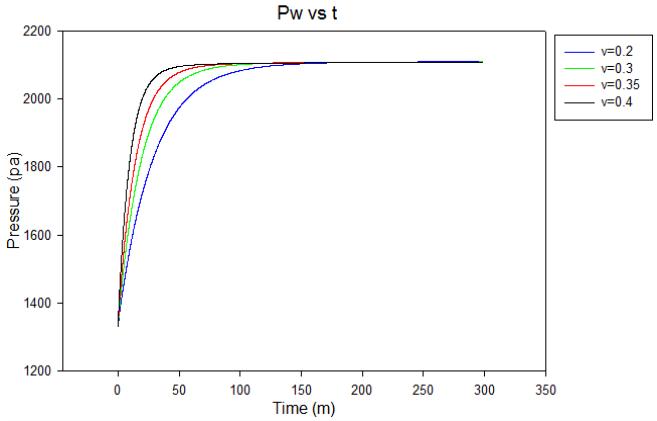

Figure 4.6: Brain tissue interstitial pressure for different brain tissue Poisson's ratio v.

4.3.2. Effects of Varying Brain Water Permeability and Viscosity

The water permeability and viscosity are varied within the range of 1.0×10^{-15} to 5.0×10^{-15} m^2 and 0.72×10^{-3} to 1.0×10^{-3} Pa.s, respectively. It should be noted that water viscosity depends on the value of body temperature, thus, the range in consideration is

for the body temperature between 27 to 37°C. Meanwhile, the human brain water permeability is in the order of 10^{-15}, thus, the range chosen is for the sake of parameter evaluation. Further investigation of a suitable value will be the subject of future work.

Figure 4.7 and 4.9 show the variation of brain tissue displacement with time for different water permeability and viscosity. Meanwhile, Figure 4.8 and 4.10 show the variation of brain tissue interstitial pressure for different water permeability and viscosity. From these figures, there are no significant changes in both brain tissue displacement and interstitial pressure when varying the water transport parameters. This finding shows that these parameters may not significantly affect brain oedema formation, unless these values are changed drastically. However, the range of values considered are within acceptable range for human.

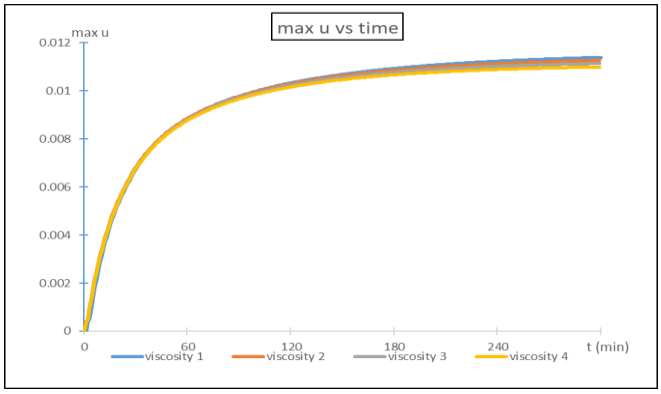

Figure 4.7: Brain tissue displacement for different water permeability k_w.

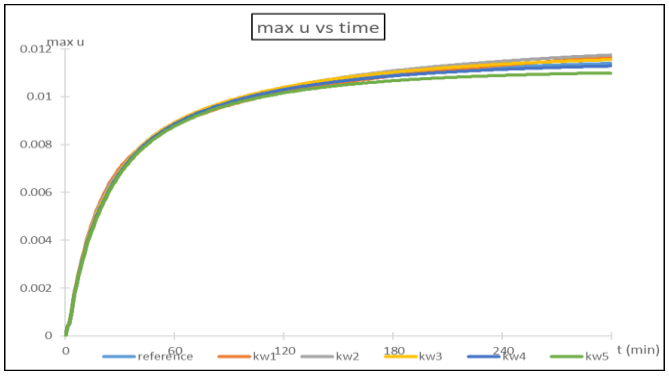

Figure 4.8: Brain tissue interstitial pressure for different water permeability k_w.

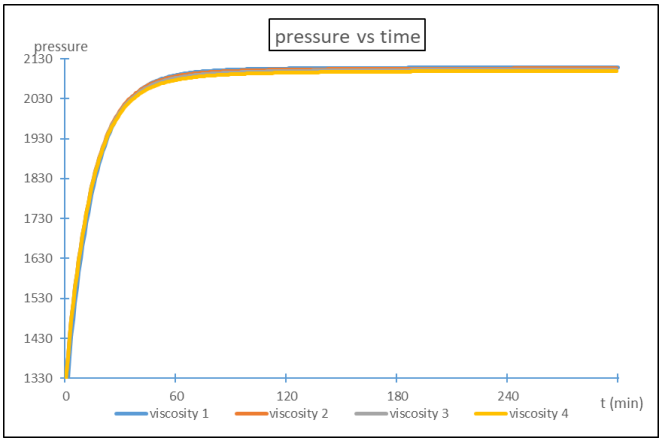

Figure 4.9: Brain tissue displacement for different water viscosity μ_w.

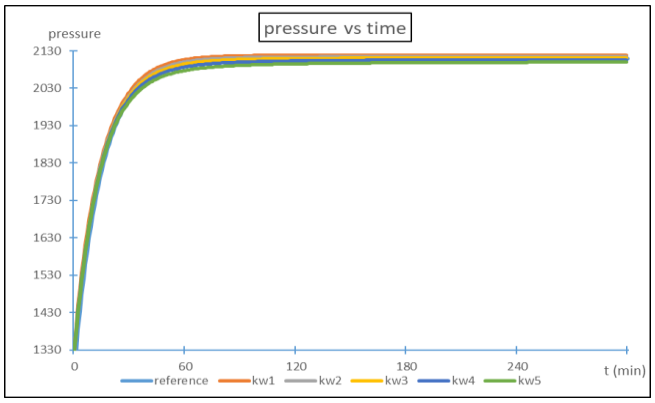

Figure 4.10: Brain tissue interstitial pressure for different water viscosity μ_w.

4.4. Discussion

In this study, it is found that the brain tissue mechanical properties greatly affect the formation of brain oedema. These properties are the brain tissue Young's modulus and Poisson's ratio. Study done by [40] on the stiffness of brain tissue during transient ischaemic injury using ultrasound elastography found that brain oedema may be determined by the changes in the brain stiffness. Another study by [41] suggested that brain tissue elasticity decreases as a result of the brain structural loss after ischaemia. These findings suggested that brain tissue mechanical properties are important in determining the development of brain oedema.

In this model, brain tissue mechanical properties have been assumed to be linearly elastic. Linear elastic assumption has been used because the brain tissue displacement

during brain tissue swelling is assumed to be very small as compared to other pathophysiological cases, for example, traumatic brain injury [42].

On the other hand, when varying the brain tissue water permeability and viscosity, there are no significant changes on the brain tissue displacement and interstitial pressure. Even though these parameters seem to not affect brain oedema formation directly, interstitial water diffusion in the porous brain structure does play an important role in determining the region of brain tissue affected by ischaemia. Water diffusion in the tissue has been extensively used in the assessment of the cell membrane integrity in pathological brain. To effectively assess the water transport properties in the brain, the model requires a modification to include water diffusion equation, as has been done, for example, in [43]. However, it should be noted that water diffusion in the brain tissue depends on the porosity and interstitial space volume, which all depends on the brain tissue mechanical properties [44]. Modification of the model are necessary to include the effect of water diffusion, which will be dealt in the future.

4.5. Conclusion

The model presented here is used to understand brain oedema formation after ischaemia-reperfusion, which has four important parameters related to the brain mechanical and fluid transport properties. However, only the brain mechanical properties, namely the Young's modulus and Poisson's ratio, have significant effects on the progression of brain oedema and interstitial pressure, while the fluid transport properties, which are the water permeability and viscosity do not significantly affect brain oedema formation.

Chapter 5: Conclusion and future work

5.1. Conclusion

This research project studies the formation of brain oedema after ischaemia-reperfusion by developing a mathematical model based on poroelasticity. Three important findings can be concluded, namely: (1) the brain oedema depends on the brain tissue mechanical properties such as Young's modulus and Poisson's ratio, but not on the fluid properties such as interstitial fluid permeability and relative compressibility; (2) the brain oedema severity depends on the size and location of the stroke infarct; and (3) a new mathematical model developed using asymptotic expansion homogenization (AEH) allows the incorporation of the brain capillary distribution on the evaluation of brain oedema.

5.2. Future Works

Based on this research, three future works are suggested, as follows: (1) the new model using asymptotic expansion homogenization can be validated using brain capillary distribution data, which can be obtained from our collaborator from Oxford University; (2) the brain tissue swelling model can be further validated using patient-specific geometry developed from medical imaging data from UMMC; and (3) hierarchical poroelastic model is in development to completely model the brain porous structure assuming extracellular fluid and blood filling the pores (double porosity).

References

[1] C. Ayata and A. H. Ropper, "Ischaemic brain oedema," Journal of Clinical Neuroscience, vol. 9, pp. 113-124, Mar 2002.

[2] W. Hacke, S. Schwab, M. Horn, M. Spranger, M. DeGeorgia, and R. vonKummer, "'Malignant' middle cerebral artery territory infarction - Clinical course and prognostic signs," Archives of Neurology, vol. 53, pp. 309-315, Apr 1996.

[3] J. I. Frank, "Large Hemispheric Infarction, Deterioration, and Intracranial-Pressure," Neurology, vol. 45, pp. 1286-1290, Jul 1995.

[4] M. J. Mohamed Mokhtarudin and S. J. Payne, "Mathematical model of the effect of ischemia–reperfusion on brain capillary collapse and tissue swelling," Math. Biosci., vol. 263, pp. 111-120, 2015.

[5] L. Soinne, S. Sundararajan, and D. Strbian, "Malignant Hemispheric Infarction Diagnosis and Management by Hemicraniectomy," Stroke, vol. 45, pp. E185-E187, Sep 2014.

[6] R. Nau, "Osmotherapy for elevated intracranial pressure - A critical reappraisal," Clinical Pharmacokinetics, vol. 38, pp. 23-40, Jan 2000.

[7] X. F. Yang, L. Wen, F. Shen, G. Li, R. Lou, W. G. Liu, et al., "Surgical complications secondary to decompressive craniectomy in patients with a head injury: a series of 108 consecutive cases," Acta Neurochirurgica, vol. 150, pp. 1241-1248, Dec 2008.

[8] D. Bereczki, M. Liu, G. F. do Prado, and I. Fekete, "Cochrane report - A systematic review of mannitol therapy for acute ischemic stroke and cerebral parenchymal hemorrhage," Stroke, vol. 31, pp. 2719-2722, Nov 2000.

[9] N. J. Abbott, A. A. Patabendige, D. E. Dolman, S. R. Yusof, and D. J. Begley, "Structure and function of the blood-brain barrier," Neurobiol Dis, vol. 37, pp. 13-25, Jan 2010.

[10] J. J. Donkin and R. Vink, "Mechanisms of cerebral edema in traumatic brain injury: therapeutic developments," Curr Opin Neurol, vol. 23, pp. 293-9, Jun 2010.

[11] M. A. Biot, "General theory of three-dimensional consolidation," J. Appl. Phys., vol. 12, pp. 155-164, 1941.

[12] Z. Taylor and K. Miller, "Reassessment of brain elasticity for analysis of biomechanisms of hydrocephalus," Journal of Biomechanics, vol. 37, pp. 1263-1269, Aug 2004.

[13] B. Tully and Y. Ventikos, "Cerebral water transport using multiple-network poroelastic theory: application to normal pressure hydrocephalus," J. Fluid. Mech., vol. 667, pp. 188-215, 2011.

[14] J. C. Vardakis, B. J. Tully, and Y. Ventikos, "Exploring the Efficacy of Endoscopic Ventriculostomy for Hydrocephalus Treatment via a Multicompartmental Poroelastic Model of CSF Transport: A Computational Perspective," Plos One, vol. 8, Dec 31 2013.

[15] Y. Yang and G. A. Rosenberg, "Blood-brain barrier breakdown in acute and chronic cerebrovascular disease," Stroke, vol. 42, pp. 3323-8, Nov 2011.

[16] S. Hakim, J. G. Venegas, and J. Burton, "The physics of the cranial cavity, hydrocephalus, and normal pressure hydrocephalus: Mechanical interpretation and mathematical model," Surg. Neurol., vol. 5, pp. 187-210, 1976.

[17] K. P. Cosgrove, C. M. Mazure, and J. K. Staley, "Evolving knowledge of sex differences in brain structure, function and chemistry," Biol. Psychiat., vol. 62, pp. 847-855, 2007.

[18] A. Smillie, I. Sobey, and Z. Molnar, "A hydroelastic model of hydrocephalus," J. Fluid Mech., vol. 539, pp. 417-443, 2005.

[19] R. A. Zimmerman, L. T. Bilaniuk, D. Bruce, C. Dolinskas, W. Obrisi, and D. Kuhl, "Computed tomography of pediatric head trauma: Acute general cerebral swelling," Radiology, vol. 126, pp. 403-408, 1978.

[20] M. C. Papadopoulos and A. S. Verkman, "Aquaporin water channels in the nervous system," Nat. Neurosci., vol. 14, pp. 265-277, 2013.

[21] Z. Taylor and K. Miller, "Reassessment of brain elasticity for analysis of biomechanisms of hydrocephalus," J. Biomech., vol. 37, pp. 1263-1269, 2004.

[22] F. Liu, S. S. Lollis, S. Ji, K. D. Paulsen, A. Hartov, and D. W. Roberts, "Model-based estimation of ventricular deformation in the cat brain," Med. Image. Comput. Comput. Assist. Interv., vol. 12(Pt 2), pp. 308-315, 2009.

[23] S. M. Nestor, R. Rupsingh, M. Borrie, M. Smith, V. Accomazzi, J. L. Wells, et al., "Ventricular enlargement as a possible measure of Alzheimer's disease progression validated using the Alzheimer's disease neuroimaging initiative database," Brain, vol. 131, pp. 2443-2454, 2008.

[24] S. K. Kyriacou, C. Davatzikos, S. J. Zinreich, and R. N. Bryan, "Nonlinear elastic registration of brain images with tumor pathology using a biomechanical model," IEEE Trans Med. Imag., vol. 18, pp. 580-592, 1999.
[25] H. K. Kimelberg, N. B. Nestor, and P. J. Feustel, "Inhibition of release of taurine and excitatory amino acids in ischemia and neuroprotection," Neurochem Res, vol. 29, pp. 267-74, Jan 2004.
[26] T. Nagashima, T. Shirakuni, and S. I. Rapoport, "A two-dimensional, finite element analysis of vasogenic brain edema," Neurol. Med. Chir., vol. 30, pp. 1-9, 1990.
[27] T. Tourdias, N. Mori, I. Dragonu, N. Cassagno, C. Boiziau, J. Aussudre, et al., "Differential aquaporin 4 expression during edema build-up and resolution phases of brain inflammation," J. Neuroinflamm., vol. 8, pp. 143-160, 2011.
[28] M. C. Papadopoulos, G. T. Manley, S. Krishna, and A. S. Verkman, "Aquaporin-4 facilitates reabsorption of excess fluid in vasogenic brain edema," FASEB J., vol. 18, pp. 1291-1293, 2004.
[29] J. J. Donkin and R. Vink, "Mechanisms of cerebral edema in traumatic brain injury: Therapeutic developments," Curr. Opin. Neurol., vol. 23, pp. 293-299, 2010.
[30] M. J. Mokhtarudin and S. J. Payne, "The study of the function of AQP4 in cerebral ischaemia-reperfusion injury using poroelastic theory," Int J Numer Method Biomed Eng, vol. 33, Jan 2017.
[31] F. Cassot, F. Lauwers, C. Fouard, S. Prohaska, and V. Lauwers-Cances, "A novel three-dimensional computer-assisted method for a quantitative study of microvascular networks of the human cerebral cortex," Microcirculation, vol. 13, pp. 1-18, Jan 2006.
[32] R. J. Shipley and S. J. Chapman, "Multiscale modelling of fluid and drug transport in vascular tumours," Bull Math Biol, vol. 72, pp. 1464-91, Aug 2010.
[33] W. K. El-Bouri and S. J. Payne, "Multi-scale homogenization of blood flow in 3-dimensional human cerebral microvascular networks," J Theor Biol, vol. 380, pp. 40-7, Sep 7 2015.
[34] S. W. Su, M. Catherall, and S. Payne, "The influence of network structure on the transport of blood in the human cerebral microvasculature," Microcirculation, vol. 19, pp. 175-87, Feb 2012.
[35] R. Penta and D. Ambrosi, "The role of the microvascular tortuosity in tumor transport phenomena," J Theor Biol, vol. 364, pp. 80-97, Jan 7 2015.
[36] R. Penta and J. Merodio, "Homogenized modeling for vascularized poroelastic materials," Meccanica, vol. 52, pp. 3321-3343, 2017.
[37] I. d. Pena, C. Borlongan, G. Shen, and W. Davis, "Strategies to extend thrombolytic time window for ischemic stroke treatment: An unmet clinical need," J. Stroke, vol. 19, pp. 50-60, 2017.
[38] M. J. Mohamed Mokhtarudin and S. J. Payne, "The study of the function of AQP4 in cerebral ischaemia–reperfusion injury using poroelastic theory," Int. J. Numer. Meth. Bio., vol. 33, 2017.
[39] M. J. Mohamed Mokhtarudin, A. Shabudin, and S. Payne, "Brain tissue swelling during ischaemia-reperfusion: 2D finite element analysis using poroelasticity," presented at the 4th International Conference on Science, Engineering & Environment (SEE), Nagoya, Japan, 2018.
[40] Z. S. Xu, R. J. Lee, S. S. Chu, A. Yao, M. K. Paun, S. P. Murphy, et al., "Evidence of changes in brain tissue stiffness after ischemic stroke derived from ultrasound-based elastography," J. Ultrasound Med., vol. 32, pp. 485-494, 2013.
[41] A. Martin, E. Mace, R. Boisgard, G. Montaldo, B. Theze, M. Tanter, et al., "Imaging of perfusion, angiogenesis, and tissue elasticity after stroke," J. Cereb. Blood Flow Metab., vol. 32, pp. 1496-1507, 2012.
[42] M. J. Mohamed Mokhtarudin and S. Payne, "Investigating the Importance of Ionic Concentration on Ischaemic Cerebral Tissue Swelling using Donnan Equilibrium," presented at the MEIbioeng16, University of Oxford, United Kingdom, 2016.
[43] M. Sarntinoranont, X. Chen, J. Zhao, and T. H. Mareci, "Computational model of interstitial transport in the spinal cord using diffusion tensor imaging," Annals. Biomed. Eng., vol. 34, pp. 1304-1321, 2006.
[44] A. R. A. Khaled and K. Vafai, "The role of porous media in modeling flow and heat transfer in biological tissues," Int. J. Heat Mass Transfer, vol. 46, pp. 4989-5003, 2003.